PCCP

Accepted Manuscript

ROYAL SOCIETY OF CHEMISTRY

www.rsc.org/pccp

Physical Chemistry Chemical Physics
CREATED USING THE RSC LaTeX PCCP ARTICLE TEMPLATE – SEE www.rsc.org/electronicfiles FOR DETAILS
ARTICLE TYPE www. rsc.org/xxxxxx | XXXXXXXX

Iron near edge X-ray spectroscopy at aqueous-membrane interfaces

Wenjie Wang,[a] Ivan Kuzmenko,[b] and David Vaknin*[a]

Employing synchrotron X-ray scattering, we systematically determine the absorption near-edge spectra (XANES) of iron in its ferrous (Fe^{2+}) and ferric (Fe^{3+}) states both as ions in aqueous solutions and as they bind to form a single layer to anionic templates that consist of carboxyl or phosphate groups at aqueous/vapor interfaces. While the XANES of bulk iron ions show that the electronic state and coordination of iron complexes in the bulk are isotropic, the interfacial bound ions show a signature of a broken inversion-symmetry environment. The XANES of Fe^{2+} and Fe^{3+} in the bulk possess distinct profiles however, upon binding they practically exhibit similar patterns. This indicates that both bound ions settle into a stable electronic and coordination configuration with an effective fractional valence (for example, $Fe^{+[2+\nu]}$, $0 < \nu < 1$) at charged organic templates. Such two dimensional properties may render interfacial iron, abundant in living organisms, a more efficient and versatile catalytic behavior.

1 Introduction

It is well established that iron ions in ferrous (Fe^{2+}) and ferric (Fe^{3+}) states can form various complexes in aqueous solutions.[1] A host of coordination compounds of trivalent and divalent iron have been characterized in the context of chemical and biological systems showing that complexed iron ions play an important role as active centers.[2] Consequently, structure and specification of iron complexes in aqueous solutions is of great importance and relevant to various disciplines such as geochemistry, mineralogy and biology. In its ferrous state, Fe^{2+} can behave as an electron donor, while in its ferric state, Fe^{3+} can be an acceptor rendering iron unique roles that have been exploited in the evolution of life, for example, its function in heme as a catalyst for reducing and oxidizing molecules and as an electron carrier.[3,4] Determining the ferrous/ferric state in situ and in real time is a challenge yet to be accomplished. However, ion-specific monitoring techniques, such as, Mössbauer effect,[5] and near L-edge and K-edge soft and hard X-ray spectroscopy techniques keep progressing, in particular, the latter ones, with the advances in synchrotron X-ray spectroscopic techniques. Unlike the Mössbauer effect method which is limited to γ-emitting nuclei, the X-ray absorption near-edge spectroscopy (XANES) techniques can be applied to practically any ion.[6–9]

Direct observation and determination of physical and chemical states of Fe^{3+} and Fe^{2+} ions near a charged or charge-neutral monolayer are highly relevant to biomineralization processes exemplified by a particular species of magnetotactic bacteria, *Magnetospirillum magneticum* AMB-1, which are capable of synthesizing single nanocrystals of magnetite Fe_3O_4 within intracellular magnetosomes.[10,11] The nucleation, formation and growth of the magnetites are observed both in vivo and in vitro in the carboxyl- and hydroxyl-enriched regions of the membrane protein, Mms6, that has been isolated from *Magnetospirillum magneticum* AMB-1.[10] Much effort has been dedicated to understand the processes of the transport and aggregation of ferric and ferrous ions into the bacteria's magnetosomes, the very beginning stages of the biomineralization. In earlier studies, we have employed Langmuir monolayers consisting of carboxyl or phosphate moieties in the form of a two-dimensional template to emulate the active iron-binding interfaces of the magnetosomes.[12–14] Mostly, a multi-layer of iron (hydr)oxides, rather than a single-molecule thick layer of ferrous and ferric ions at the interface of Langmuir monolayer, are observed under the aqueous surface monolayers,[14,15] resulting from the pre-existing iron complexes in buffer solutions.[1,13,14] In this study, iron solutions were prepared at low pH (2.5 for Fe(III), 3.5 for Fe(II)) to significantly suppress the concentration of Fe(III) (hydr)oxide (colloidal and suspended) aggregates[13] and to minimize the oxidation rate of Fe(II) ions,[16] in an attempt to form a single bound layer of iron to an organic template. These measures allow us to explore a single layer of ferrous and ferric iron ions bound to two dimensional templates of a carboxyl or phosphate moieties prepared by Langmuir monolayers on aqueous solutions by employing surface XANES and complement the results with X-ray reflectivity and near-total-reflection fluorescence techniques. Specular X-ray reflectivity (XR) and angular-dependent near-total-reflection fluorescence spectroscopy techniques are used to determine the distribution of surface-bound iron ions. Whereas the X-ray fluorescence and reflectivity provide good estimates on bound-ions per molecule and their spatial distribution, surface XANES probes the effective valence (i.e., electronic configuration) and coordination of the ions at the interface. The XANES spectra are characterized by three major features:1. pre-edge, 2. main ab-

[a] *Ames Laboratory and Department of Physics and Astronomy, Iowa State University, Ames, Iowa 50011, USA. ; E-mail: vaknin@ameslab.gov*
[b] *X-ray Science Division, Advanced Photon Source, Argonne National Laboratory, Argonne, Illinois 60439, USA.*

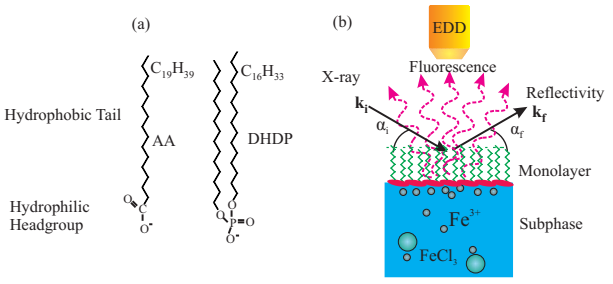

Fig. 1 (a) Schematic representations of AA and DHDP molecules. The length of the hydrocarbon chain (tail) are estimated as ~ 24 and 20 Å in terms of the number of CH_2 groups (1.27 Å per CH_2 group) along the chain axis.[26,27] (b) The demonstration of setup for surface reflectivity and fluorescence measurements (also used for XANES).

sorption crest, and 3. spectra shape above the absorption edge. Quantitative interpretation of XANES spectra is challenging, as they are affected by formal valence, coordination, site geometry and ligand type. Qualitative analysis by comparison to atoms in control systems can thus provide useful insights.[8,9] For iron, as is the case for transition metals in general, the presence of a pre-edge signal is indicative of quadrupole transition of $1s \rightarrow 3d$ by virtue of p and d hybridization that is commonly caused by a broken inversion-symmetry in non-centrosymmetric structures.[17] To demonstrate qualitative and quantitative ion binding to the monolayers we employ X-ray near-total-reflection fluorescence[12,13,18–21] and X-ray reflectivity (XR) techniques[22–25] to the same samples that are subsequently used for XANES experiments.

2 Experimental Methods

Monolayers of arachidic acid (AA) and dihexadecyl phosphate (DHDP) providing a negatively monovalent charge upon deprotonation were each deposited on aqueous surfaces of $FeCl_3$ or $FeCl_2$ solutions, where the surface charge and the solubility of iron are regulated by pH levels.[13] Arachidic-acid (AA, $C_{20}H_{40}O_2$, CAS No. 506-30-9) and dihexadecyl phosphate (DHDP, $C_{32}H_{67}O_4P$, CAS No. 2197-63-9) were purchased from Sigma-Aldrich Co. Ion bulk concentrations were prepared using solutions of $FeCl_3 \cdot 6H_2O$ (ferric chloride hexahydrate) and $FeCl_2$ (ferrous chloride anhydrous), were obtained from Sigma-Aldrich, and chemicals used without further purification. All iron solutions were prepared at 1 mM. Ultrapure water (Millipore, Milli-Q, and NANOpure, Barnstead; resistivity 18.1 MΩcm) was used for all subphase preparations, and HCl solution was used to acidify the pure water before dissolving iron salts and to further adjust the pH of iron solutions (pH 2.5 for $FeCl_3$ and 3.5 for $FeCl_2$). This protocol of solution preparation has been used to minimize oxidation of Fe^{2+}. As a further measure to reduce oxidation the $FeCl_2$ solutions were prepared in containers that were continuously purged over with argon gas. Pure AA or DHDP was each dissolved in 3:1 chloroform/methanol solution and spread at gas/water interfaces in a thermostatic, solid Teflon Langmuir trough kept at constant temperature (20**°C**). Compression of the monolayer, at a rate of ~ 1 Å^2 per molecule per minute, was started 10-15 minutes after spreading to allow for evaporation of the solvent, and surface-pressure was recorded with a microbalance using a filter-paper Wilhelmy plate. To minimize radiation damage due to the formation of radicals and ions and to reduce background scattering from air, the encapsulated trough was continuously purged with water saturated helium during the X-ray experiments. X-ray scattering and spectroscopy studies were conducted on the Liquid Surface Spectrometer at the Advanced Photon Source (APS), beam-line 9ID-C. The highly monochromatic beam (7.7 keV of wavelength $\lambda = 1.6102$ Å for fluorescence and reflectivity; and tunable in the 7.1-7.3 keV range for XANES measurements) was selected by a downstream cryogenically cooled Si(111) double crystal monochromator. The angle of incidence at the liquid sample was set by a Ge(111) steering crystal located on the liquid surface diffractometer. The XANES signals, in reflection-fluorescence mode, were collected with a Vortex energy dispersive detector (EDD) that is also used for the fluorescence measurements. X-ray fluorescence signals from the films as a function of incident beam angle α_i (proportional to Q_z at these small angles, $Q_z = 4\pi \sin\alpha_i/\lambda$, α_i being X-ray incident angle with respect to the interface), are used to determine quantitatively the density of specific ions that accumulate at the interface.[12,13,18–20] XR is displayed as a function of Q_z yielding the electron density (ED) profile normal to the interface from a parametrized ED profile.[25] A graphic illustration of the molecular structure of AA and DHDP, and the experimental configuration for XANES, fluorescence and reflectivity measurements is shown in Fig.1.

3 Results and Discussion

3.1 Iron adsorption as a single layer

Figure 2 shows fluorescence intensities integrated over the Fe K_α characteristic emission line as a function of Q_z from $FeCl_3$ and $FeCl_2$ solutions without and with a monolayer. The intensity of the fluorescence signal from the bare surface of the ion-solution (I_b) from the bulk iron concentration (n_b) is given by[13,21]

$$I_b(\alpha_i) = C\,|t(\alpha_i)|^2\, D(\alpha_i)\, g(\alpha_i) A_0 n_b, \qquad (1)$$

whereas the fluorescence intensity from the monolayer-covered surface has two contributions, one from bound ion at the interface (of surface density n_s), I_s, and the other from

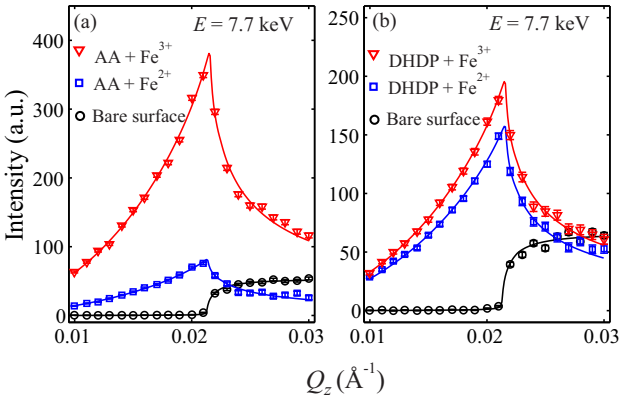

Fig. 2 Florescence intensity as a function of Q_z for iron bulk solution (1 mM) with bare surface and ion-enriched surface. Each data point is integrated over range from 6.2 to 6.6 keV containting exclusively the Fe $K\alpha$ emission line ($K_\alpha \approx 6.4$ keV). Each error bar represents one standard deviation arising from counting statistics. The circular symbols represent the bulk signal from 1 mM of $FeCl_2$ solutions in the absence of the monolayer, which is indistinguishable from that of 1 mM of $FeCl_3$, and is profile-fit with Eqn.(1). The square and triangle symbols represent the surface signal after the subtraction of bulk signal from the whole florescence signal from 1 mM $FeCl_3$ or $FeCl_2$ solutions in the presence of the monolayer and are profile-fit with Eqn.(2).

bulk ions I_b, (i.e., $I_s + I_b$), given by [13,21]

$$I_s(\alpha_i) = C\,|t(\alpha_i)|^2\, g(\alpha_i) A_0 n_s \exp[-|z_{\rm ion}|/D(\alpha_i)] \qquad (2)$$

where, C is a scale factor that accounts for beam intensity and EDD efficiency, A_0 is the average molecular area (≈ 20Å^2 for AA and ≈ 40Å^2 for DHDP), $t(\alpha_i)$, $D(\alpha_i)$, and $g(\alpha_i)$ are the transmission function, the penetration depth normal to the interface and a geometrical correction,[29] respectively. $z_{\rm ion}$ is the position of the ion-enriched layer with respect to $z = 0$ at the gas/monolayer interface.The analysis of the spectra and its α_i dependence (Fig. 2) yield the number of bound iron ions per carboxyl or phosphate headgroup, $N_{\rm Fe}$, at the interface.[18–20] Particularly, for $\alpha_i > \alpha_c$, α_c being the critical angle for total reflection, where $|z_{\rm ion}/D(\alpha_i)| \ll 1$, to a good approximation,[20]

$$N_{\rm Fe} = n_s A_0 = \left[\frac{I_s(\alpha_i)}{I_b(\alpha_i)}\right] D(\alpha_i) A_0 n_b \qquad (3)$$

The analysis of the fluorescence signals is summarized in Table 1 showing that the number of bound Fe^{3+} per molecule ($N_{\rm Fe}$) is more than 1/3 per head group, the amount necessary to neutralize a fully charged surface. Also the binding of Fe(III) is almost independent of the charge density at the interface, namely independent of either AA or DHDP template, suggestive of tethered ferrihydrides complexes formation at the interface, which is consistent with previous reports

Table 1 Number of iron nuclei per molecule (DHDP or AA) extracted from the analysis of the X-ray fluorescence measurements as described in the text.

Binding ratio	Fe(III)	Fe(II)
$N_{\rm Fe}$ per AA (±15%)	0.60	0.13
$N_{\rm Fe}$ per DHDP (±15%)	0.46	0.42

on the binding of Fe^{3+} and La^{3+} to similar templates.[12,13] On the other hand, for Fe(II) there are 0.13 Fe per AA at nearly charge-neutral interface and 0.42 per DHDP. This is consistent with the fact that simple electrostatic forces dominate the accumulation of Fe(II) at these two interfaces. The position of the ion layer is found to be at $z_{\rm ion} \approx 20$ Å contiguous to or within the headgroup strata as it is also found in the XR analysis discussed below.

The fluorescence results are corroborated by the X-ray reflectivity measurements. Measured X-ray reflectivity curves (R) normalized to the calculated reflectivity of an ideally flat water surface(R_F; R/R_F) are shown in Fig. 3(a) for monolayers of AA and DHDP on iron solutions as indicated. The ED profiles for the surface monolayer are modeled as two-layers; one contains the headgroup, and the other the hydrocarbon-chain tail.[25] The effective-density model[22,28] that allows for large, uncorrelated interfacial roughness was adopted to construct interfacial ED profiles. The solid lines shown in Fig. 3(b) are the best-fit model calculations obtained from the electron density profiles across the interfaces using Parratt's exact recursive method,[24,28], in which the continuous model ED profile is approximated by parsing it into a stack of thin slabs. More details can be found in Tolan's monograph or Supporting Information.[22,28] Qualitatively, for both ion solutions, the ED-enhanced regions on the ED profiles can be readily associated with the headgroup, which is higher than for a monolayer that is spread on pure water,[12–14] evidence for ion binding within a few angstroms of the headgroup region. Furthermore, the density of bound Fe(III) to AA monolayer is significantly higher than that of Fe(II), while the density of the two bound ions to DHDP are within experimental uncertainty the same, and in good agreement with the observations from the fluorescence measurements.

3.2 XANES of Fe^{2+} and Fe^{3+} in bulk solution

To systematically test our method of collecting XANES in reflection mode from an aqueous surface, we start by discussing the XANES of bulk ions and proceed to the surface for comparison. The XANES spectra from bulk can be obtained at a fixed Q_z value above the critical angle for total scattering ($Q_c = 0.0218$ Å^{-1}) for which the penetration depth of the beam is a few microns. Here, we keep Q_z constant at 0.05

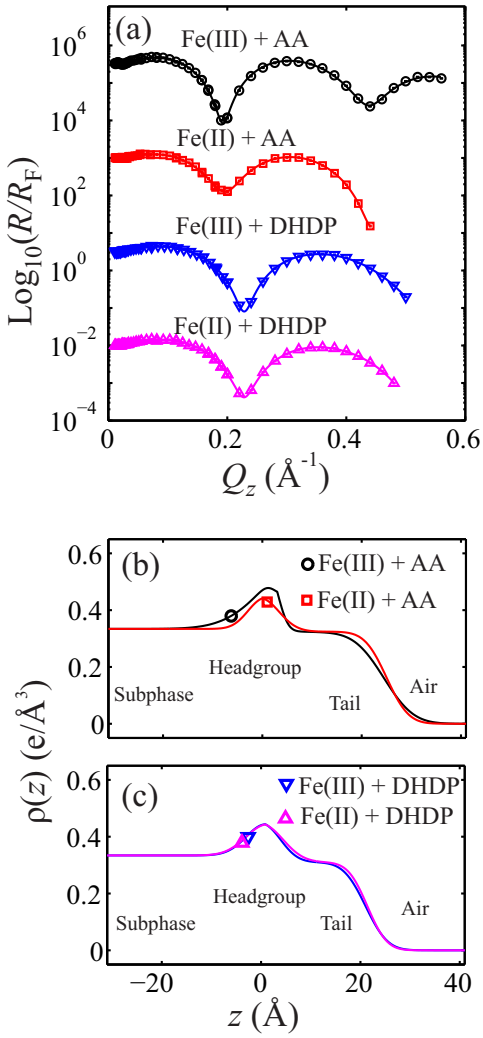

Fig. 3 (a) Normalized X-ray reflectivity from four different combinations of two monolayers (AA or DHDP) with either ferric or ferrous ion containing subphases. The symbols represent the experimental data. Solid lines through these symbols are best curve-fit. The data and curves are shifted vertically for clarity. (b) and (c) ED profiles simulated by the best-fit parameters corresponding to (a). From the left to the right, the ED profiles are approximately divided into four regions, i.e. subphase, headgroups and tails of the monolayer, and gas phase. Position $z = 0$ has been shifted to the center of head group for better display.

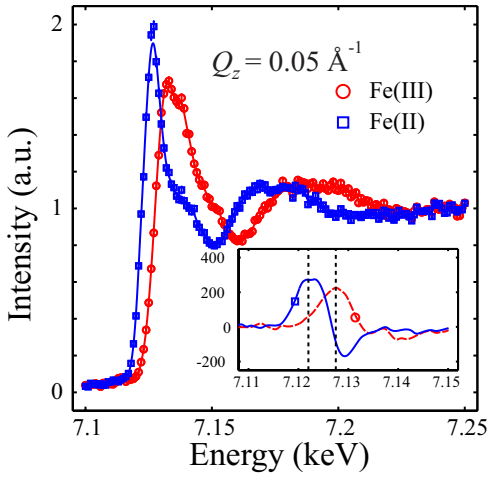

Fig. 4 X-ray absorption K-edge spectra and corresponding derivatives (inset) showing the difference in edge spectra (maxima) for Fe^{3+} and Fe^{2+} in the bulk solution with bare surface.Two vertical dashed lines are positioned at 7.1220 and 7.1275 keV, respectively.

$Å^{-1}$ at which the x-ray beam penetrates to approximately 5 μm into the bulk of the solution. The XANES spectra for Fe^{3+} and Fe^{2+} in bulk solution, shown in Fig. 4, is obtained by integrating over the fluorescence signal consisting exclusively of K_α emission line of iron. These results are the first to be obtained from Fe ions in reflection mode and they compare very well with previous results obtained in transmission mode.[30] The main absorption lines for Fe(II) and Fe(III) are separated by a 5 eV chemical shift that is better visualized in the derivative of the absorption spectra with respect to the incident photon energy, as shown in the inset Fig. 4. The spectra does not exhibit any evidence of a pre-edge signal indicating very little *d*-*p* hybridization of iron with its nearest neighbors, evidence for a highly symmetric environment around the two different ions in the bulk. Based on analysis of the Fe(III) and Fe(II) spectra in aqueous solutions it has been proposed that the highly symmetric complexes consist of $[Fe(H_2O)_6]^{3+}$ and $[Fe(H_2O)_6]^{2+}$, respectively.[30]

3.3 Interfacial XANES of iron

To measure the interfacial XANES from bound ions we keep the incident beam below the critical angle for total reflection. In this mode the penetration depth of the evanescent wave at the surface is less than 100 Å. The surface XANES from both monolayers is obtained at $Q_z = 0.018 Å^{-1}$ with a penetration depth ~ 80 Å as shown in Fig. 5.

The spectra from the interfacial bound ions differ markedly from those of bulk displaying nearly indistinguishable shape for Fe(II) and Fe(III) for both, AA and DHDP. This may in-

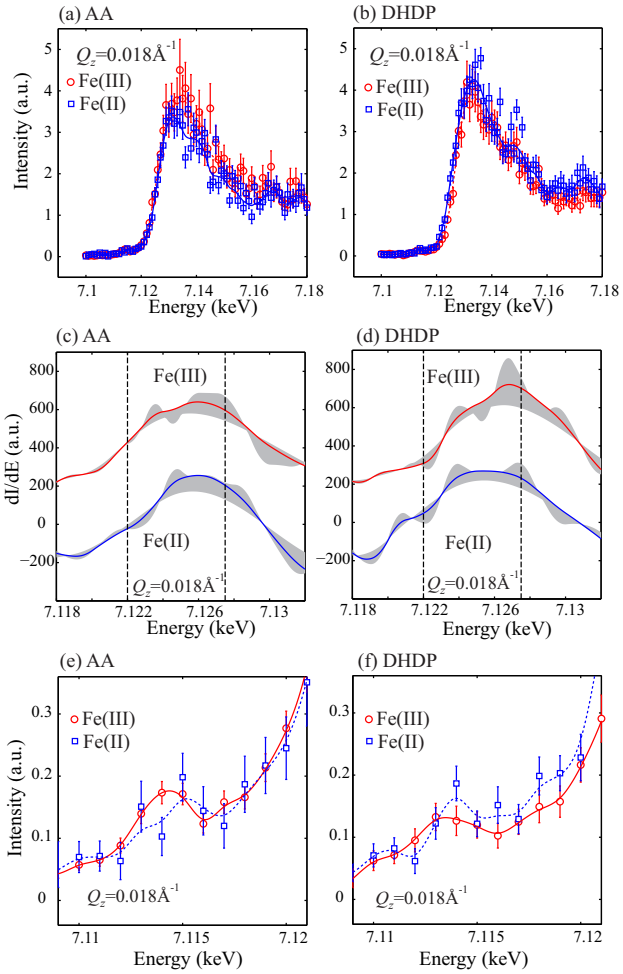

Fig. 5 X-ray absorption K-edge spectra (upper panels), corresponding derivatives of edge spectra (middle panels), and pre-edge structure (lower panels) for Fe^{3+} and Fe^{2+} at the interface. (a), (c) and (e) are for AA; (b), (d) and (f) are for DHDP. The vertical dotted lines are peak positions for aqueous bulk Fe^{2+} and Fe^{3+} as shown in the inset of Fig. 4. XANES intensities are normalized to the higher energy end of the spectra (7.19 – 7.20 keV). (Prior to the normalization, the spectra intensities at higher energy end for Fe^{2+} need to be scaled up by 5.9 and 1.3 times for the AA and DHDP monolayers to be comparable to the corresponding Fe^{3+} spectra, respectively.) (c) and (d) derivatives of XANES spectra intensity ($I(E)$) with respective to photon energy (E) (curves shifted vertically by 400 arb. units apart for clarity) in terms of the cubic splines that best-profile-fit the XANES data (weighted by the detector counting error). The gray area provides the associated uncertain regions for less stringent requirement for data smoothing.[31] (e) and (f) the pre-edge structure in the XANES spectra, prior to the main absorption rise edge, which is much suppressed in the spectra for the bulk XANES of aqueous iron ions.

dicate a common stable electronic configuration and coordination at charged organic templates for bound iron. Furthermore, the derivatives of the spectra with respect to photon energy, while showing differences between the two ions, exhibit a common peak intermediate between that the free Fe(II) and Fe(III) ions in the bulk. This is suggestive of coexistence of both ions at the interface, or, this may indicate uniform fractional valence (for example, $Fe^{+[2+\nu]}; 0 < \nu < 1$) and/or unusual coordination. We note that these experiments were conducted at various collecting data rates and exposure to photons to allow for monitoring any time dependent effects or possible chemical modification by X-ray radiation dose and were found to be reproducible. Another observation in the surface XANES of iron is the emergence of the pre-edges in the presence of AA and DHDP, for both Fe(II) and Fe(III) as shown in the inset to Fig. 5. This, we argue, is expected as interfaces naturally break inversion symmetry. Unlike in bulk, interfacial bound iron ion is bonded to a head group on one side and surrounded by water molecules on the other resulting in a symmetry and environment changes that bring about the pre-edge.[28]

4 Conclusions

XANES from monovalent ions (i.e., Cs^+) at a charged Langmuir monolayer by scanning photon energy of the X-ray reflectivity at fixed Q_z values[20] has been reported, and subsequently has been employed to ferrihydride aggregates that are bound to a Langmuir monolayer.[14] In particular, it has been shown that the spectra from these aggregates is consistent with Fe^{3+}, which was also confirmed in a recent independent study by various methods including XANES.[15] In this study, we have adjusted the solution conditions (i.e., pH) so no aggregates are formed in the solution as evidenced in our XR that shows a single layer of ions is bound to the charged interface. We generalize the method to obtain XANES from bulk and interfacial ions in reflection mode from charged aqueous interfaces. We show that the sensitivity of the technique in providing distinct spectra for Fe^{2+} and Fe^{3+} in bulk solutions with a 5 eV chemical shift and isotropic coordination can be achieved in this mode. The differences between the spectra above the edge indicate a different coordination for the two ions.[30] By contrast, the spectra of bound iron ions are significantly different than any of the two Fe^{2+} or Fe^{3+} in bulk solution and are nearly indistinguishable. Furthermore, they exhibit a detectable pre-edge signal that indicates the ions are not loose as in a distribution predicted by Poisson-Boltzmann theory, but chemically bound to the headgroup in the so called Stern-layer.[32] Furthermore, the interfacial XANES shown in Fig. 5 are quite similar to those obtained from Fe atoms in neuromelanin granules in a surviving neuron whereas in a dead neuron with neuromelanin aggregates the signal is more like that of

Fe^{3+}.[33] Charged biological templates are topologically similar to those explored here, we therefore hypothesize that iron or other transition metals share similar electronic configurations that render them more efficient functions as charge carriers and catalyzers in their un-aggregated forms. For instance, transition-metal phthalocyanines or porphyrins, considered as artificial light harvesting pigments, exhibit undesired exciton splitting in their electronic absorption spectra when forming dimers and higher order aggregates[34,35] prompting a search for methods to control and preserve their two dimensional assembly.[36] Such aggregation may also be related to the fact that the distribution of Fe^{2+} and $Fe^{3}+$ in zeolite based catalysts depends on Fe concentration in addition to protocol of thermal treatment.[37].

Acknowledgments

We thank R. Y. Park (Ames Laboratory, Iowa State University) for technical support at APS. The work at the Ames Laboratory was supported by the Office of Basic Energy Sciences, U.S. Department of Energy under Contract No. DE-AC02-07CH11358. Use of the Advanced Photon Source was supported by the U. S. Department of Energy, Office of Science, Office of Basic Energy Sciences, under Contract No. DE-AC02-06CH11357.

References

1 R. M. Cornell and U. Schwertmann, *The Iron Oxides: Structure, Properties, Reactions, Occurrences and Uses*, VCH Publishers: New York, NY, 1996.

2 N. Wiberg and A. F. Holleman, Editors. *Inorganic Chemistry* , chapter XXIX (*The iron Group*), Academic Press, San Diego, 2001.

3 A. G. Sykes, *Heme-Fe Proteins* in *Advances in Inorganic Chemistry* **51**, (Academic Press, San Diego, 2001).

4 K. H. Nealson and D. Saffarini, *Annu. Rev. Microbiol.* 1994, **48**, 311.

5 E. R. Bauminger, P. M. Harrison, D. Hechel, N. W. Hodson, I. Nowik, A. Treffry and S. J. Yewdall, *Biochem. J.* 1993, **296**, 709.

6 P. Glatzel and U. Bergmann, *Coordination Chemistry Reviews* 2005, **249**, 65.

7 K. M. Kemner, S. D. Kelly, B. Lai, J. Maser, E. J. O'Loughlin, D. Sholto-Douglas, Z. Cai, M. A. Schneegurt, C. F. Kulpa Jr. and K. H. Nealson, *Science* 2004, **306**, 686.

8 G. A. Waychunas, M. J. Apted and G. E. Brown Jr., *Phys. Chem. Minerals* 1983, **10**, 1.

9 I. Joly, *Synchrotron Rad.* 2003, **10**, 58.

10 A. Arakaki, J. Webb and T. Matsunaga, *J. Biol. Chem.* 2003, **278**, 8745.

11 M. Tanaka, E. Mazuyama, A. Arakaki, T. Matsunaga. *J. Biol Chem.* 2011, **286**, 6386.

12 W. Wang, R. Y. Park, A. Travesset and D. Vaknin, *Phys. Rev. Lett.* 2011, **106**, 056102.

13 W. Wang, R. Y. Park, D. M. Meyer, A. Travesset and D. Vaknin, *Langmuir* 2011, **27**, 11917.

14 W. Wang, J. Pleasants, W. Bu, R. Y. Park, I. Kuzmenko and D. Vaknin, *J. Colloid Interf. Sci.* 2012, **384**, 45.

15 D. C. F. Wieland, P. Degen, M. Paulus, M. A. Schroer, S. Bieder, C. J. Sahle, J. Möller, S. Leick, Z. Chen, B. Struth, H. Rehage and M. Tolan, *Colloids and Surfaces B: Biointerfaces* 2013, **109**, 74.

16 W. Stumm and G. F. Lee, *Ind. Eng. Chem.* 1961, **53**, 43.

17 F. de Groot, G. Vankó,and P. Glatzel *J. Phys.: Condens. Matter* 2009, **21**,104207.

18 W. B. Yun and J. M. Bloch, *J. Appl. Phys.* 1990, **68**, 1421.

19 J. Daillant, L. Bosio, J. J. Benattar and C. Blot, *Langmuir* 1991, **7**, 611.

20 W. Bu and D. Vaknin, *J. Appl. Phys.* 2009, **105**, 084911.

21 W. Wang, W. Bu, L. Wang, P. E. Palo, S. Mallapragada, M. Nilsen-Hamilton and D. Vaknin, *Langmuir* 2012, **28**, 4274.

22 M. Tolan, *X-ray scattering from soft-matter thin films*, (Springer, Germany, 1999).

23 J. Daillant and A. Gibaud, Eds. *X-ray and neutron reflectivity: principles and applications*, (Springer, Germany, 1999).

24 J. Als-Nielsen and D. McMorrow, *Elements of Modern X-ray Physics*, **2011**, John Wiely & Sons: London,2011.

25 D. Vaknin, X-ray Diffraction and Spectroscopic Techniques for Liquid Surfaces and Interfaces. In *Characterization of Materials*; Ed. Kaufmann, E. N. (John Wiley & Sons: New York, 2012) Vol. 2, 1393-1423.

26 K. Kjaer, J. Als-Nielsen, C. A. Helm, P. Tippman-Krayer and H. Möhwald, *J. Phys. Chem.* 1989, **93**, 3200.

27 Small, D. M. *The Physical Chemistry of Lipids: From Alkanes to Phospolipids*; Handbook of Lipid Research; Plenum Press: New York and London, 1986; Vol. 4, Chapter 3.

28 Supporting Information.

29 D. K. G. De Boer, *X-Ray Spectrometry* 1989, **18**, 119.

30 M. Benfatto, J. A. Solerab and J. G. Ruizb, *Chem. Phys.* 2002, **282**, 441.

31 Note: The MATLAB (MathWorks) function, *csaps*, is used to conduct the data profile-fitting, with a smoothing parameter p adjusting relative weight of *error* measure and *roughness* measure (information can be found in MathWorks spline toolbox user's guide). Here, p (weight for the error measure) is chosen at an optimized value $(1-10^{-8})$, associated with the spacing of the data points) that the splines represent the data well ($p=1$ corresponds to the case that splines go through each data point). The weight for the roughness measure $(1-p)$ is further varied from

$10^{-7} - 10^{-9}$ to check the uncertainty of the spline fitting. The gray area in (c) and (d) provides the uncertain region where the splines would rest if the requirement of the smoothness relaxes.

32 J. N. Israelachvili, *Intermolecular and Surface Forces*, (Academic Press, San-Diego, 2000).

33 S. Yoshida, A. Ektessabi and S. Fujisawa, *J. Synchrotron Rad.* 2001, **8**, 998.

34 C. C. Leznoff, A. B. P. Lever, Edts. *Phthalocyanines: Properties and Applications* **1989**, (VCH Publishers: New York) Vol. 1.

35 L.-K. Chau, C. Arbour, G. E. Collins, K. W. Nebesny, P. A. Lee, C. D. England, N. R. Armstrong and B. A. Parkinson, *J. Phys. Chem.* 1993, **97**, 2690.

36 B. W. Gregory, D. Vaknin, J. D. Gray,B. M. Ocko, T. M. Cotton and W. S. Struve, *J. Phys. Chem. B* 1999, **103**, 502.

37 M. S. Maier, A. Jentys, E. Metwalli, P. Müller-Buschbaum, and J. A. Lercher, *J. Phys. Chem. Lett.* 2011, **2**, 950.

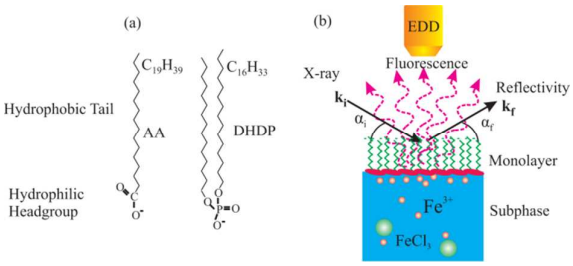

We determine the absorption near-edge spectra of iron in its ferrous and ferric states both as ions in aqueous solutions and as they bind to form a single layer to anionic templates that consist of carboxyl or phosphate groups at aqueous/vapor interfaces.